Supplementary information

Olig2 acts as an inducible barrier to in vivo astrocyte-to-neuron conversion

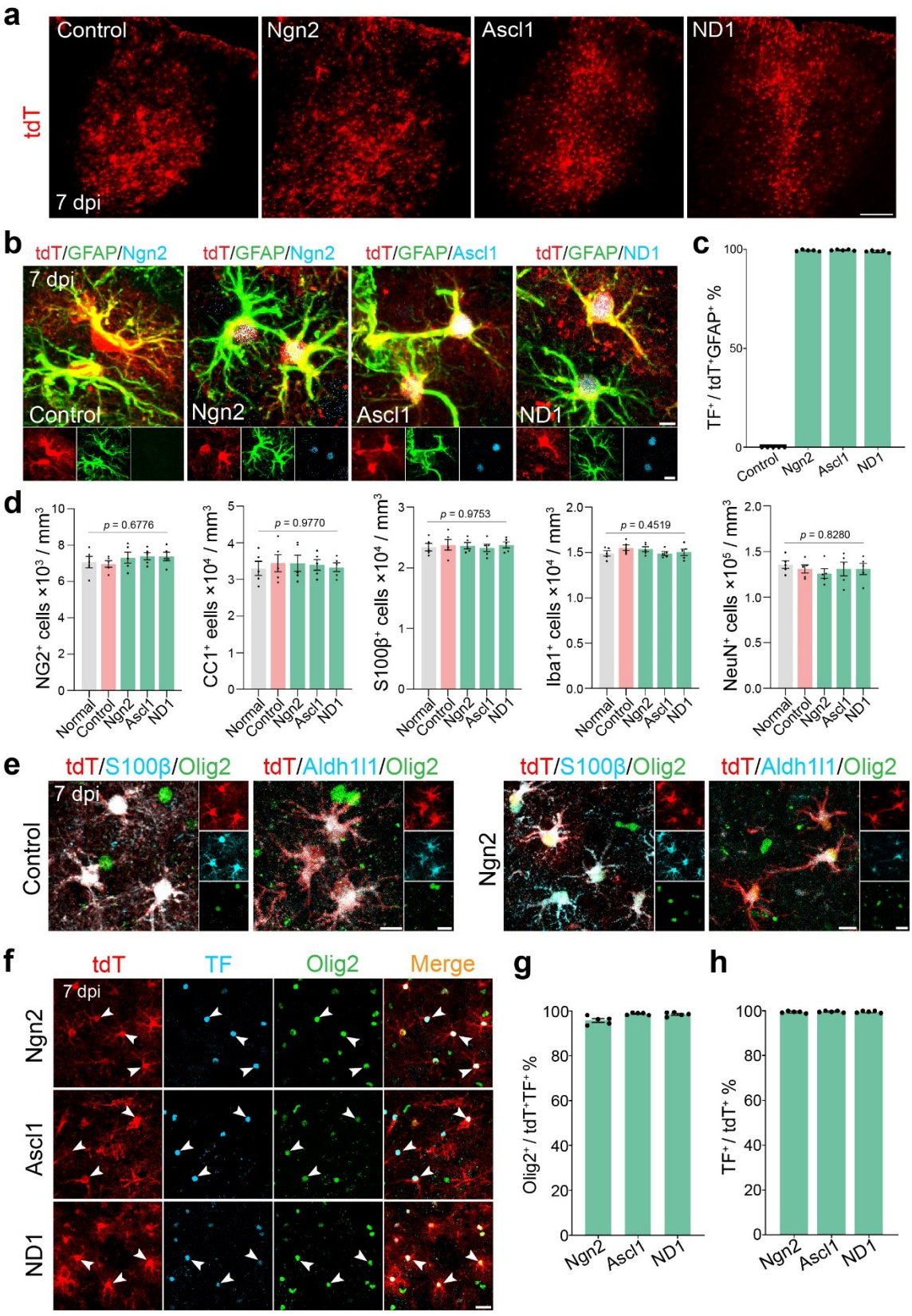

Supplementary figure 1. Olig2 upregulation in astrocytes with bHLH proneural transcription factor overexpression

a, Low-magnification images showing virus-infected regions in the cortex. Scale bar, 200 μm. **b,** Representative images showing co-expression of tdT, TFs (Ngn2, Ascl1, and NeuroD1) and GFAP (7 dpi). Scale bar, 5 μm above, 10 μm below. **c,** Quantification showing efficient overexpression of TFs in astrocytes (7 dpi); n = 5 mice per group, mean ± SD. **d,** Quantified data showing no significant cell number change of $S100\beta^+$ astrocytes, $Iba1^+$ microglia, $NeuN^+$ neurons, $NG2^+$ OPCs, and $CC1^+$ oligodendrocytes at 7 dpi; n = 5 mice per group, one-way ANOVA followed by Bonferroni's post hoc test, mean ± SD. **e,** Confocal images showing co-expression of Olig2 and astrocytic markers S100β or Aldh1l1 at 7 dpi. Scale bars, 10 μm. **f,** Representative images showing co-localization of Olig2 and Ngn2/Ascl1/ND1 in nuclei (arrowheads). Scale bar, 20 μm. **g,** Quantified data showing high level co-expression between Olig2 and Ngn2/Ascl1/ND1; n = 5 mice per group, mean ± SD. **h,** Quantification showing high level co-expression of tdT and transcription factors; n = 5 mice per group, mean ± SD.

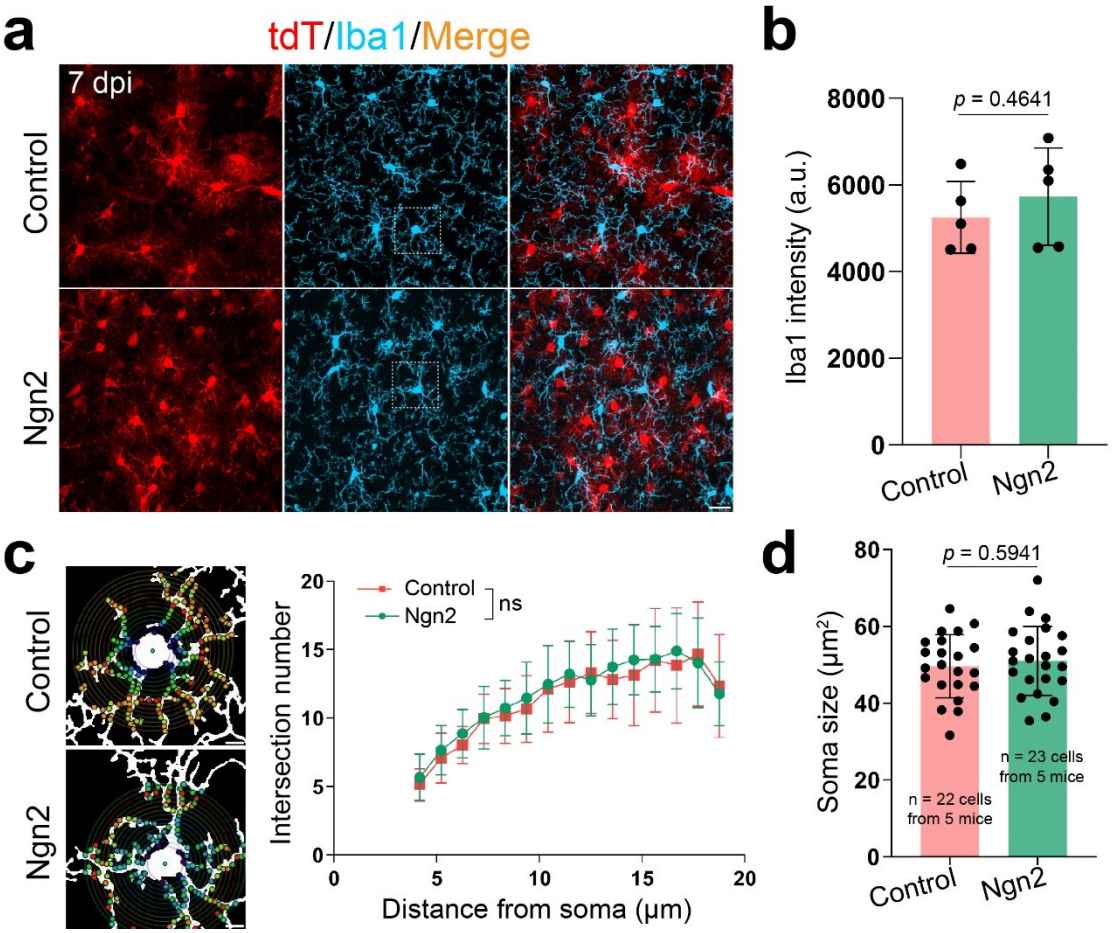

Supplementary figure 2. Ngn2 overexpression does not significantly affect

microglial reactivity

a, Confocal images showing Iba1 expression with or without Ngn2 overexpression at 7 dpi. Scale bar, 20 µm. **b,** Quantification of Iba1 fluorescence intensity showing no significant differences between groups; n = 5 mice per group, unpaired Student's t-test, mean ± SD. **c,** Sholl analysis revealing comparable microglial branching complexity between conditions; two-way repeated measure analysis of variance, mean ± SD. **d,** Quantification showing unchanged microglial soma size following Ngn2 overexpression; n = 22 cells from 5 mice with control virus overexpression and n = 23 cells from 5 mice with Ngn2 overexpression, unpaired Student's t-test, mean ± SD.

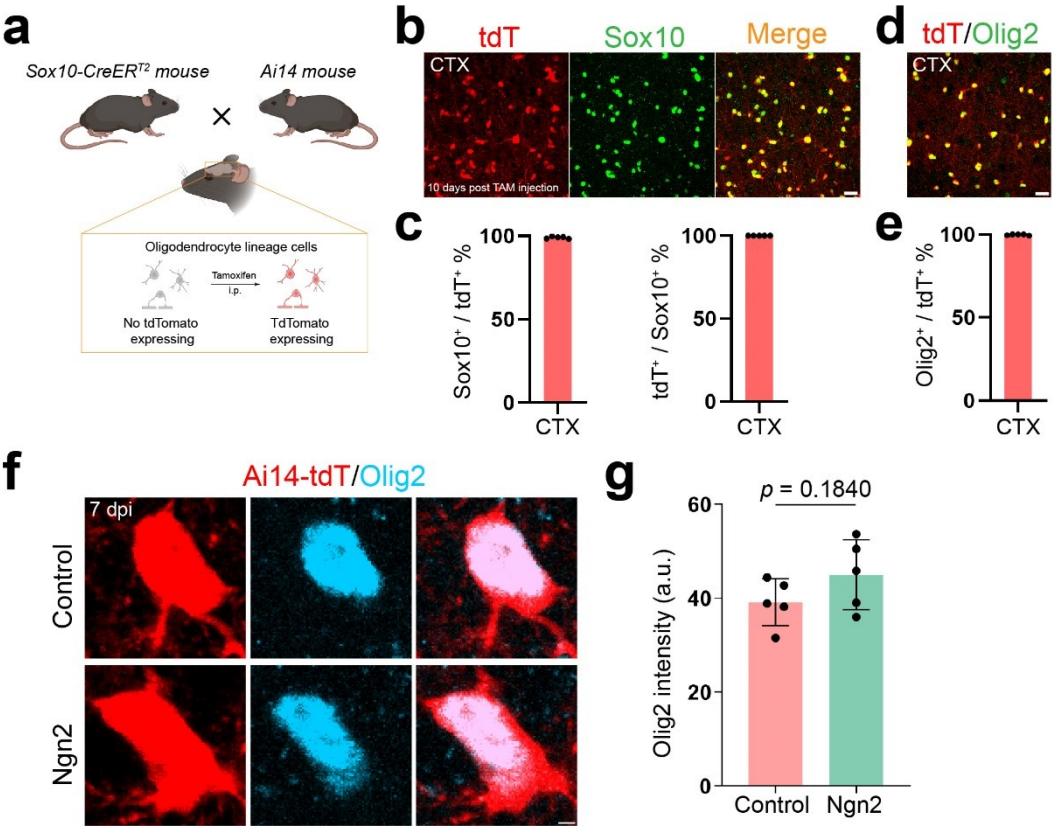

Supplementary figure 3. High specificity of tdT labeling in Sox10-CreER^{T2} × Ai14 mice

a, Schematic diagram showing the cross of Sox10-CreER^{T2} mouse and Ai14 mouse to produce the double transgenic mouse, in which oligodendrocyte lineage cells can express tdTomato after tamoxifen administration. Created in BioRender.com. Hou, KY. (https://BioRender.com/q38wdm8). **b,** Confocal images showing co-staining of tdT and SOX10 in the cortex at 10 days post tamoxifen injection. Scale bar, 20 μm. **c,** Quantified data showing high level co-expression between tdT and Sox10, indicating high specificity of tdT signal; n = 5 mice per group, mean ± SD. **d,** Typical image showing Olig2 expression in tdT$^+$ cells. Scale bar, 20 μm. **e,** Quantified data showing high expression level of Olig2 in tdT$^+$ cells; n = 5 mice per group, mean ± SD. **f,** Typical images showing Olig2 expression in tdT$^+$ oligodendrocyte lineage cells with or without Ngn2 overexpression. Scale bar, 2 μm. **g,** Quantification showing comparable Olig2 fluorescence intensity between groups; n = 5 mice per group, unpaired Student's t-test, mean ± SD.

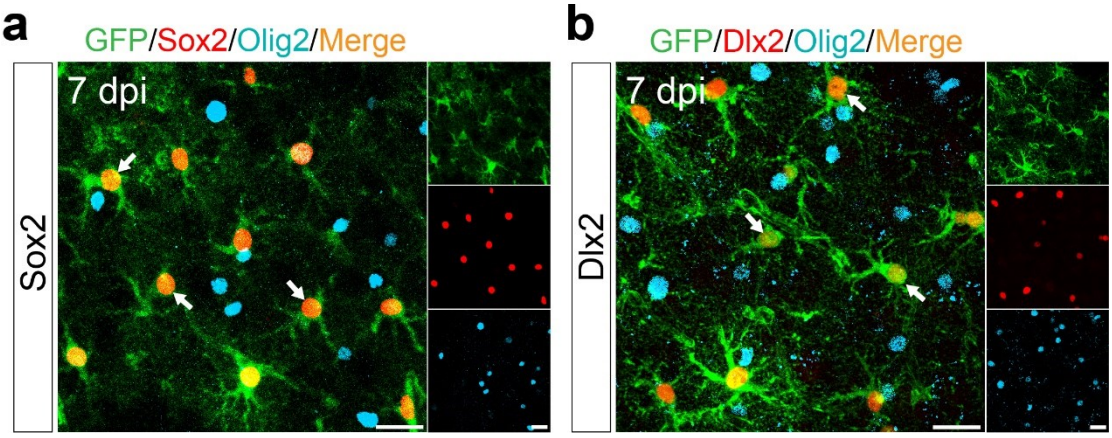

Supplementary figure 4. Non-bHLH family transcription factors Sox2 and Dlx2 do not induce Olig2 upregulation

a, Typical images showing no significant Olig2 upregulation induced by Sox2 overexpression in astrocytes (7 dpi). n = 5 mice. Scale bar, 20 μm. **b,** Representative images showing rare Olig2 upregulation with Dlx2 overexpression in astrocytes (7 dpi). n = 5 mice. Scale bar, 20 μm.

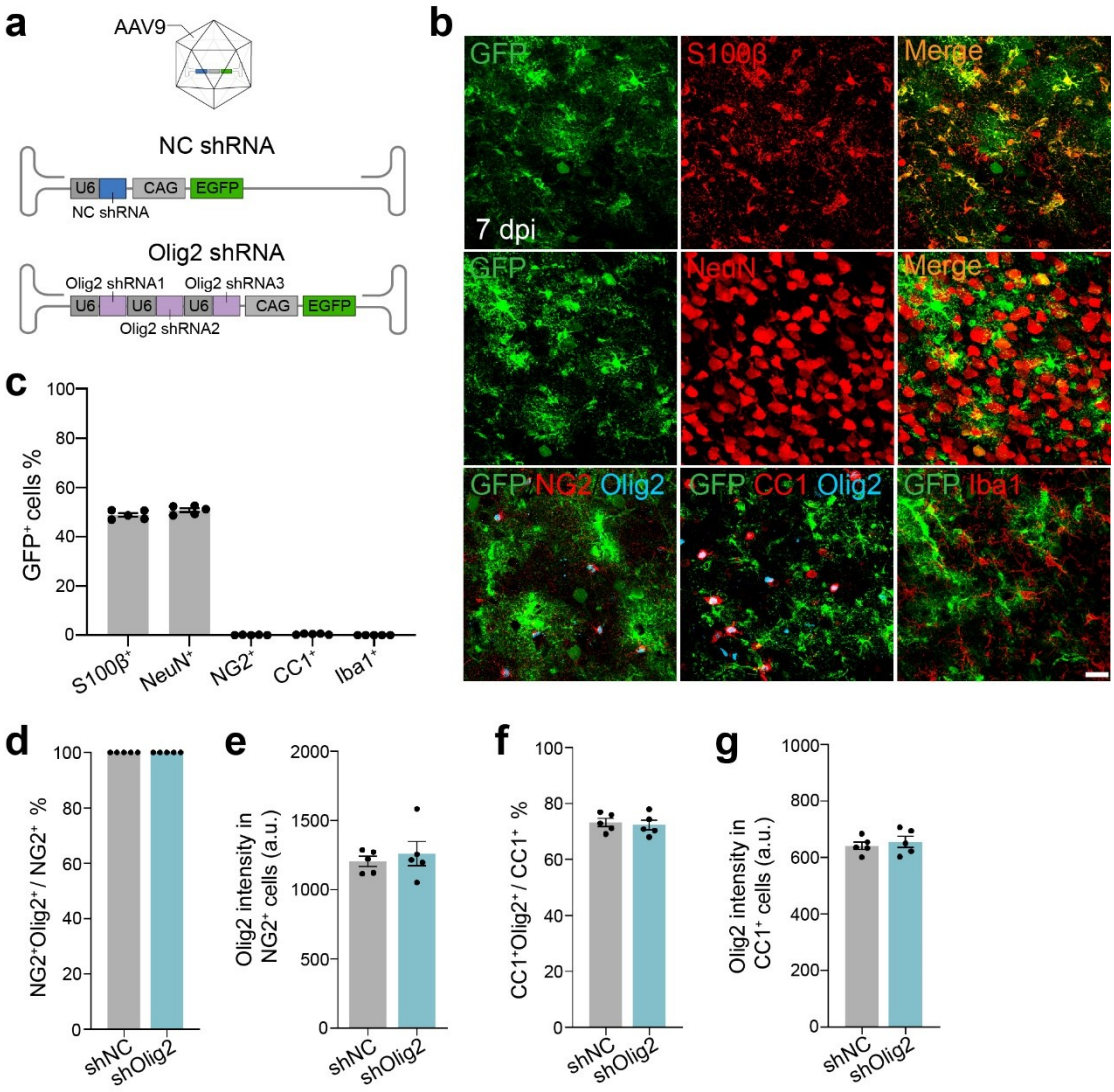

Supplementary figure 5. shRNA expression in astrocytes and neurons

a, Scheme of the universal negative control (NC) and Olig2 shRNA with EGFP for cell visualization. Created in BioRender.com. Hou, KY. (https://BioRender.com/z4rzbde). **b,** Representative images showing EGFP co-staining with S100β, NeuN, NG2/Olig2, CC1/Olig2, and Iba1 at 7 dpi. Scale bar, 20 μm. **c,** Quantified data showing shOlig2 expression in astrocytes and neurons, rarely in OPCs, oligodendrocytes and microglia; n = 5 mice per group, mean ± SD. **d-g,** Quantified data showing rare impact of shOlig2 on endogenous Olig2 expression in $NG2^+$ OPCs and $CC1^+$ oligodendrocytes, including Olig2 proportion (**d, f**) and intensity (**e, g**). Quantification of intensities in Supplementary Fig. 5e refers to data in Supplementary Fig. 5d, whereas Supplementary Fig. 5g corresponds to data in Supplementary Fig. 5f; n = 5 mice per group, mean ± SD.

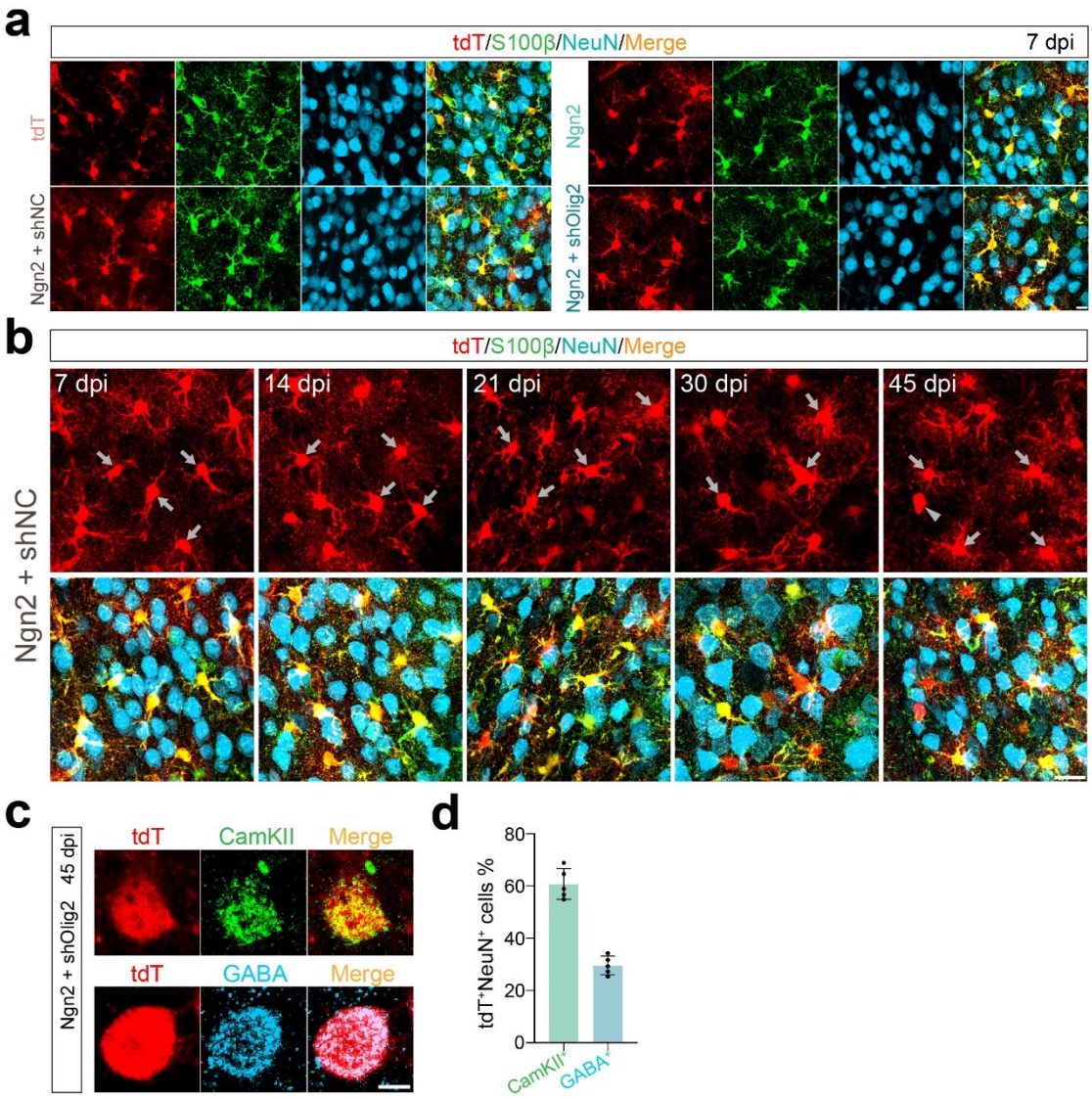

Supplementary figure 6. Most of converted neurons are excitatory

a, Representative images showing tdT co-staining with S100β and NeuN among four groups (tdT, Ngn2-tdT, Ngn2+shNC, and Ngn2+shOlig2) at 7 dpi. Note that tdT^+ cells were mostly co-localized with S100β at early time point. Scale bar, 20 μm. **b,** Immunostaining showing the morphology changes of tdT^+ cells in the Ngn2+shNC group from 7 to 45 dpi. Arrow indicating $tdT^+S100\beta^+NeuN^-$ cells, arrowhead indicating $tdT^+S100\beta^-NeuN^+$ cells. Scale bar, 20 μm. **c,** tdT and glutamatergic neuronal marker CaMKII or GABAergic neuronal marker GABA co-staining in Ngn2+shOlig2 treated mice at 45 dpi. Scale bar, 5 μm. **d,** Quantified data showing that more $CaMKII^+$ neurons were generated than $GABA^+$ neurons with Ngn2+shOlig2; n = 5 mice per group, mean ± SD.

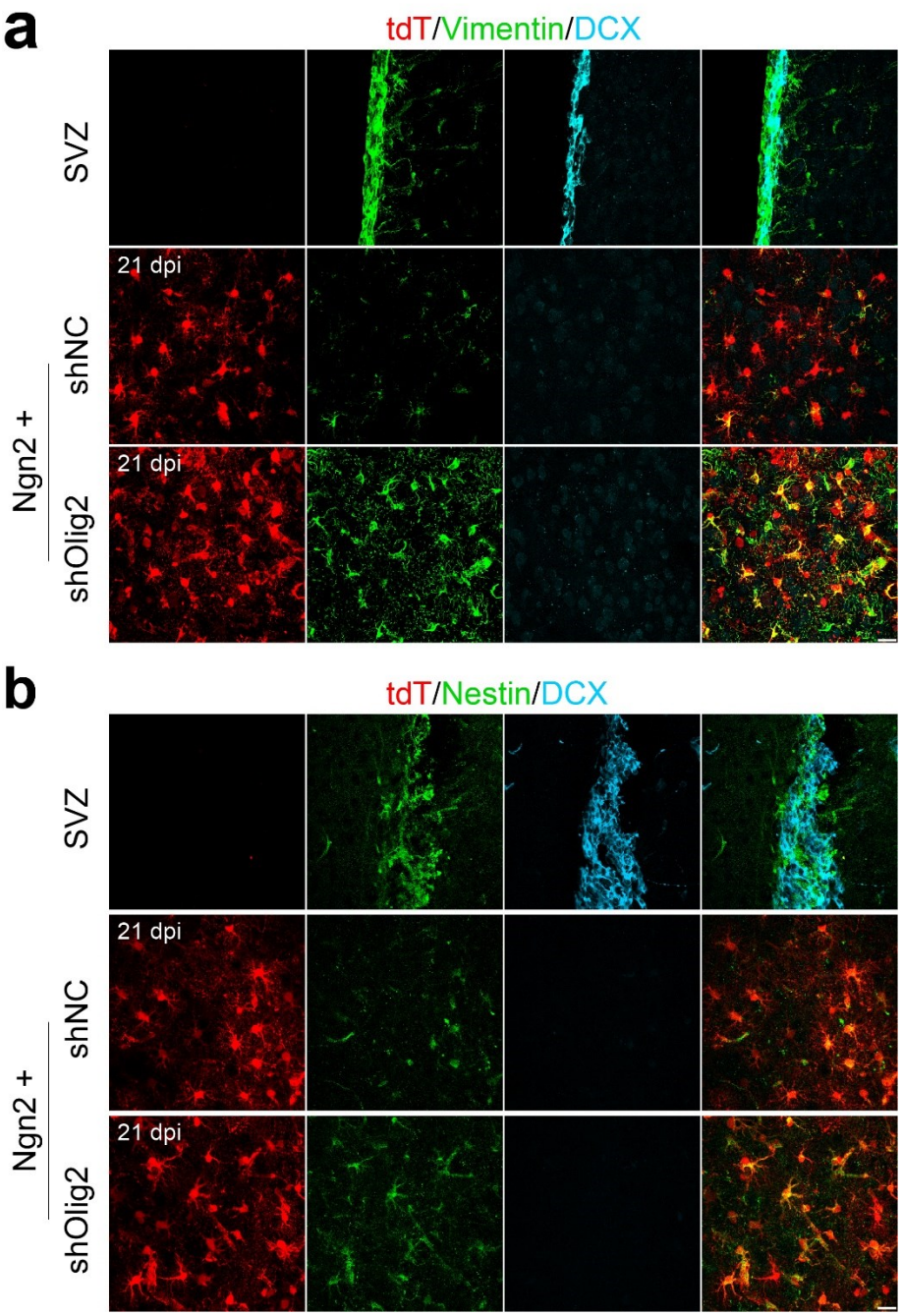

Supplementary figure 7. Olig2 knockdown does not upregulate DCX expression

a, Representative images showing co-staining of tdT, Vimentin, and DCX. Note that, While Vimentin and DCX showed robust expression in uninfected SVZ (control), Olig2 knockdown in Ngn2-overexpressing astrocytes upregulated Vimentin but not DCX. Scale bar, 20 μm. **b,** Representative images showing co-staining of tdT, Nestin, and DCX. Consistent with panel a, Nestin and DCX were highly expressed in naive SVZ, but Olig2 knockdown only upregulated Nestin (not DCX) in reprogrammed astrocytes. Scale bar, 20 μm.

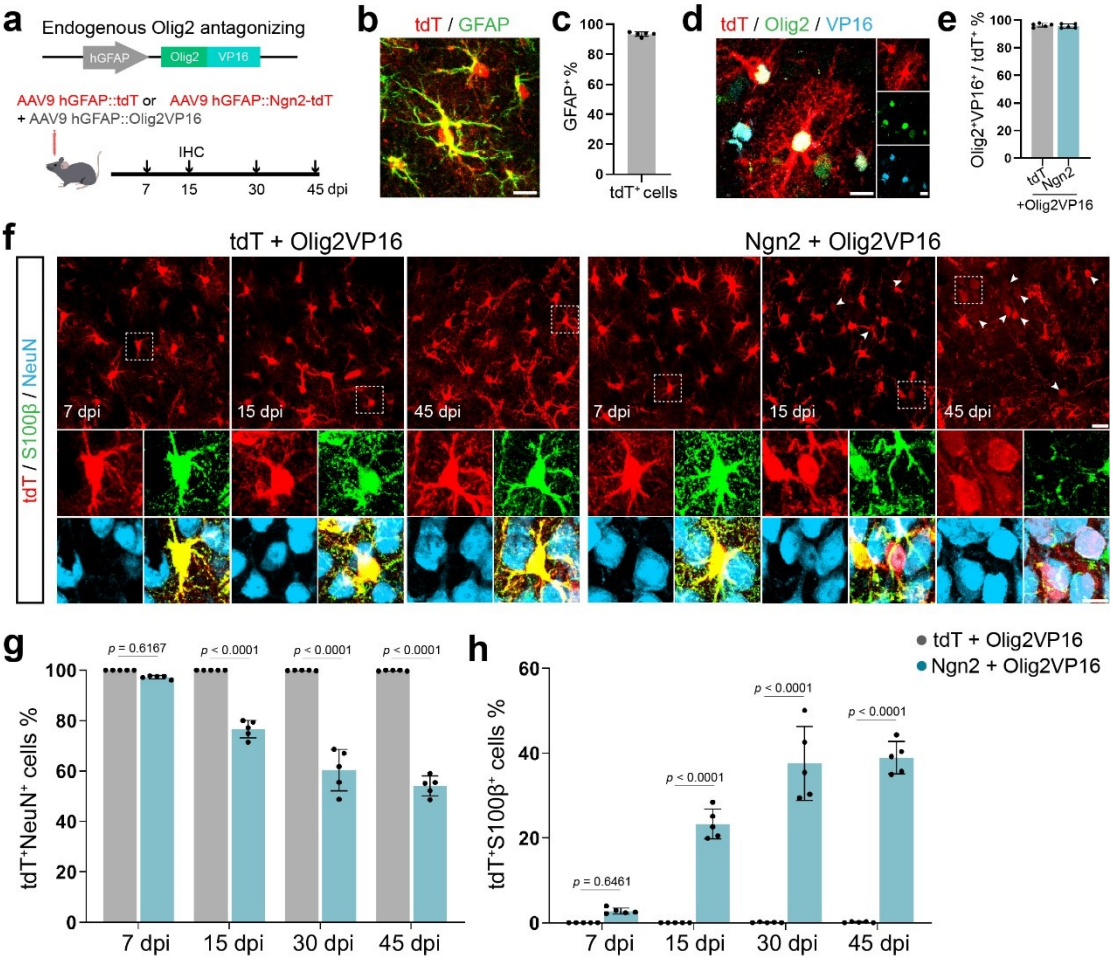

Supplementary figure 8. Olig2 acts as a repressor in AtN reprogramming

a, Scheme of the Olig2VP16 and experimental design. Created in BioRender.com. Hou, KY. (https://BioRender.com/3efgztj). **b-c,** Immunostaining and quantified data showing a high co-label rate of tdT and GFAP in AAV9 infected cells. Scale bar, 10 μm; n = 5 mice per group, mean ± SD. **d-e,** Immunostaining and quantified data showing high level co-expression of Olig2/VP16 and tdT in both groups. Scale bar, 10 μm; n = 5 mice per group, mean ± SD. **f,** Representative images showing tdT co-staining with S100β and NeuN at 7, 30, 45 dpi between the tdT+Olig2VP16 and the Ngn2+Olig2VP16 group. Dashed boxes represent the enlarged images. Scale bar, 20 μm. **g,** Quantification of the proportion of $tdT^+S100\beta^+$ cells from 7 to 45 dpi; n = 5 mice per group, unpaired Student's t-test, mean ± SD. **h,** Quantification of the proportion of tdT^+NeuN^+ cells from 7 to 45 dpi; n = 5 mice per group, unpaired Student's t-test, mean ± SD.

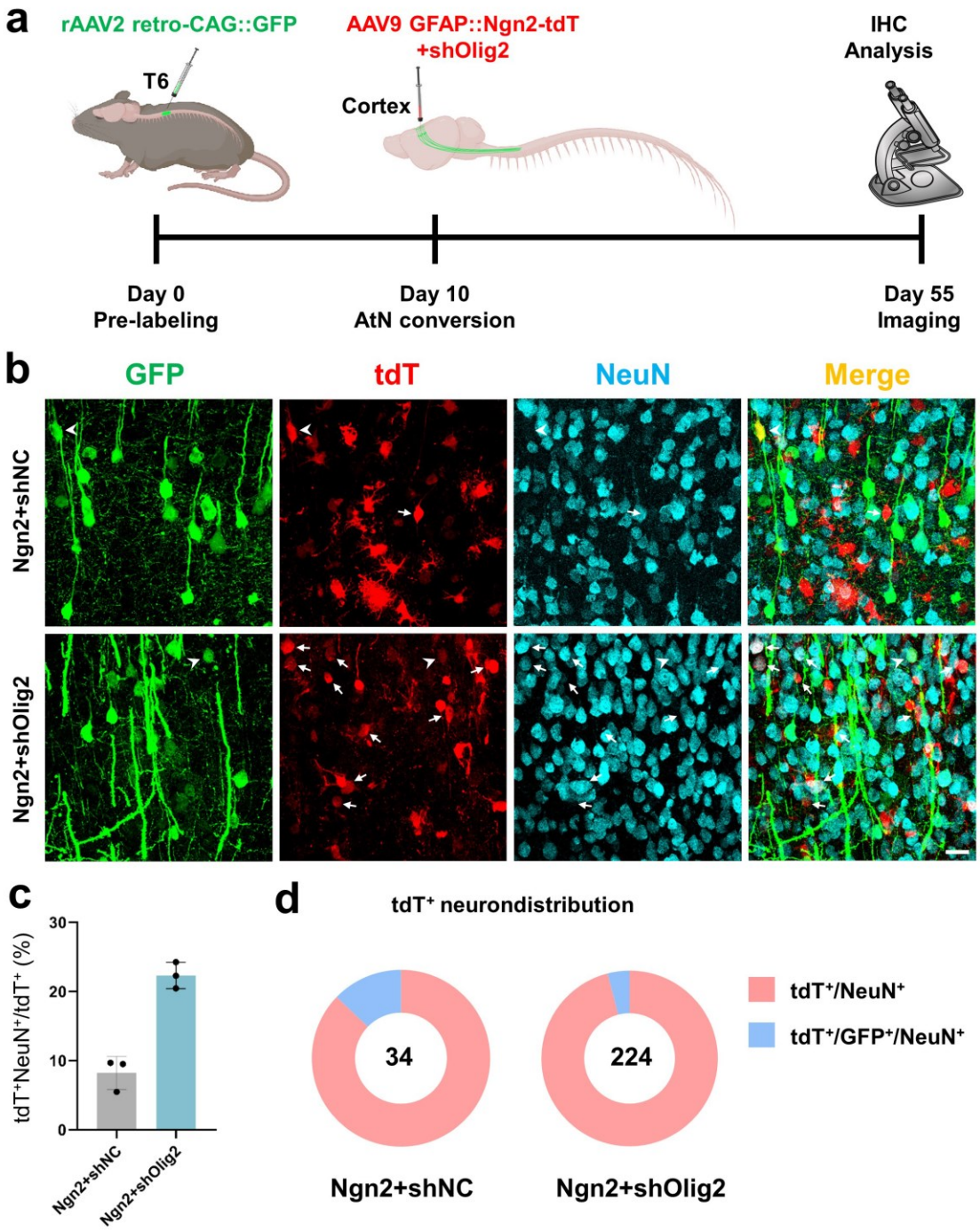

Supplementary Figure 9. AAV pre-labeling of endogenous neurons to further confirm AtN reprogramming

a, Schematic illustrating the study design: endogenous cortical neurons (green) were pre-labeled, followed by the injection of reprogramming factors (red) into the mouse cortex. T6 refers to the 6th thoracic spinal cord level. Created in BioRender.com. Hou, KY. (https://BioRender.com/ma8kpmp). **b,** Confocal images showing pre-labeled endogenous cortical neurons (GFP^+) and AAV-transduced cells (tdT^+). Arrows indicate examples of tdT^+ neurons, and the arrowhead points to neurons with dual reporters.

Scale bar, 10 μm. **c,** Bar graph depicting the percentage of tdT$^+$ neurons among total tdT$^+$ cells, reflecting reprogramming efficiency. **d,** Pie chart illustrating the distribution of tdT$^+$ neurons. The number in the center of the pie chart represents the total number of tdT$^+$ neurons (from 3 mice).

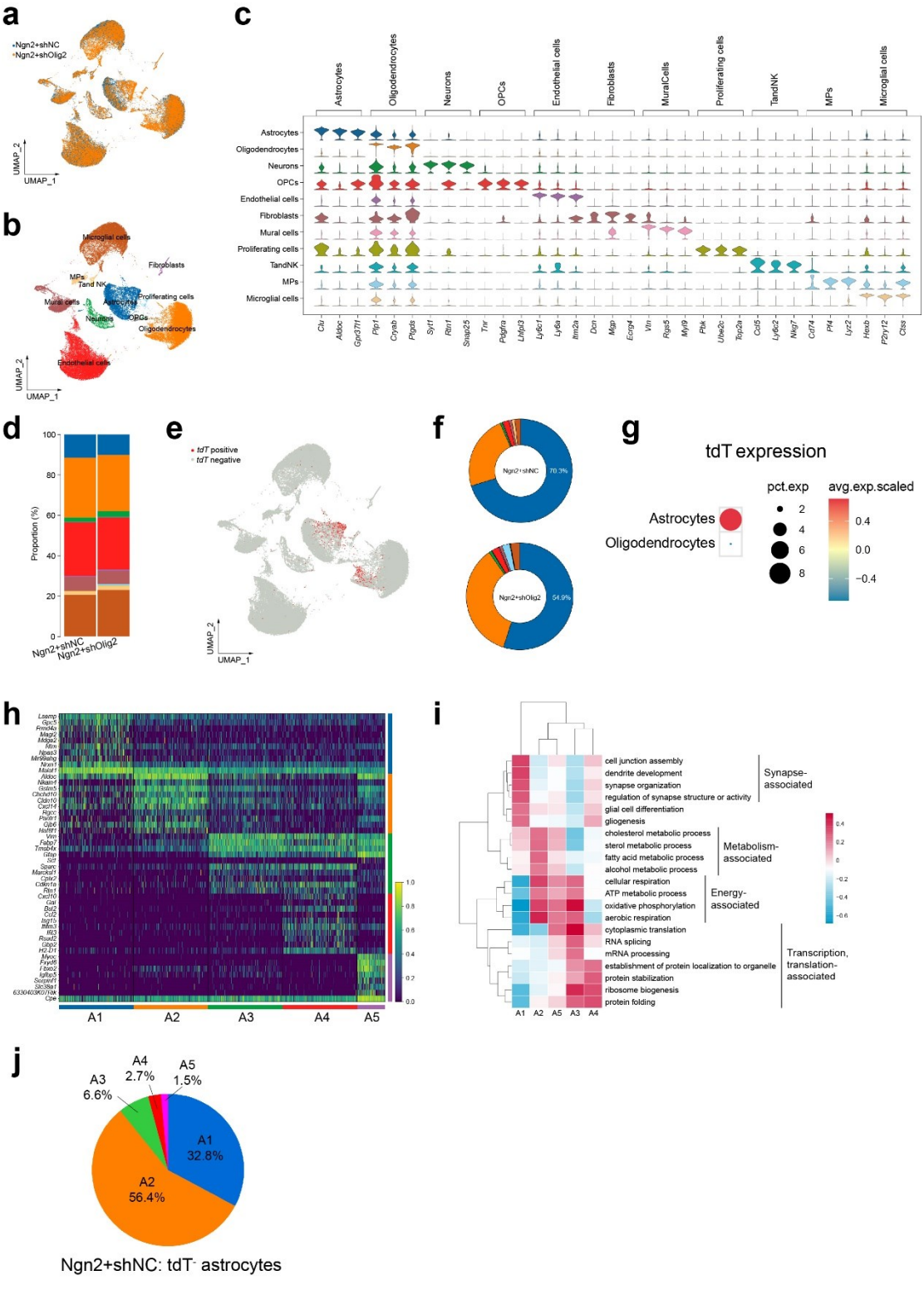

Supplementary figure 10. Cell types identification and sub-clustering of astrocytes

a, Cell clusters of the Ngn2+shNC and the Ngn2+shOlig2 groups. **b,** Unsupervised clustering of cell population. **c,** Violin plot depicting selected differentially expressed genes for each cluster. **d,** Histogram showing the percentage of different cell types in each group. **e,** TdT projection to panel b. **f,** Pie chart showing the distribution of tdT transcript in cell clusters. **g**, Dot plot showing higher tdT expression proportion and level in astrocytes compared to oligodendrocytes. **h,** Heatmap depicting the differentially expressed marker genes in different astrocyte sub-clusters. **i,** Gene set variation analysis (GSVA) showing differentially enriched pathways among astrocyte sub-clusters. **j,** Pie chart showing the proportion of five astrocytic sub-clusters among tdT^- cells in the Ngn2+shNC group.

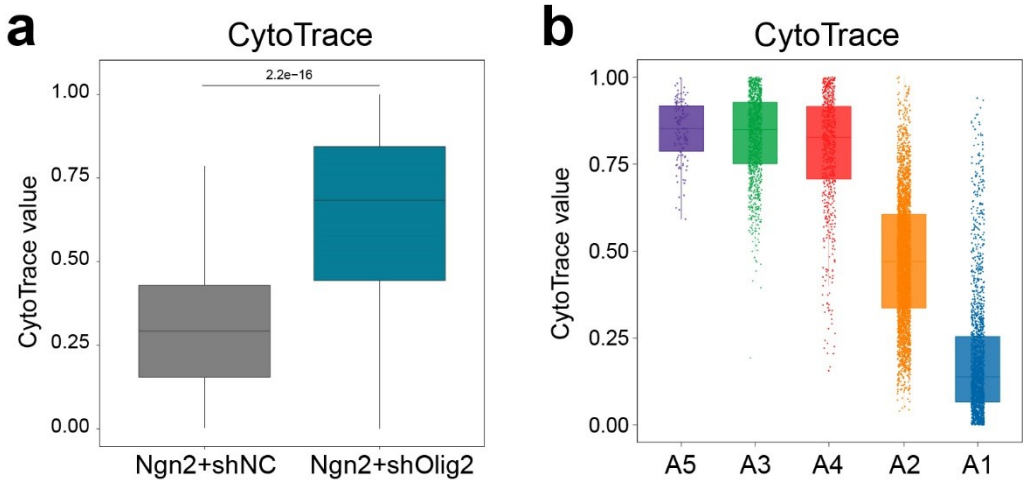

Supplementary figure 11. Higher stemness of astrocytes with Olig2 knockdown

a, CytoTrace analysis showing higher stemness of tdT^+ astrocytes in the Olig2 knockdown group. **b,** CytoTrace analysis showed higher stemness of A3 and A4.

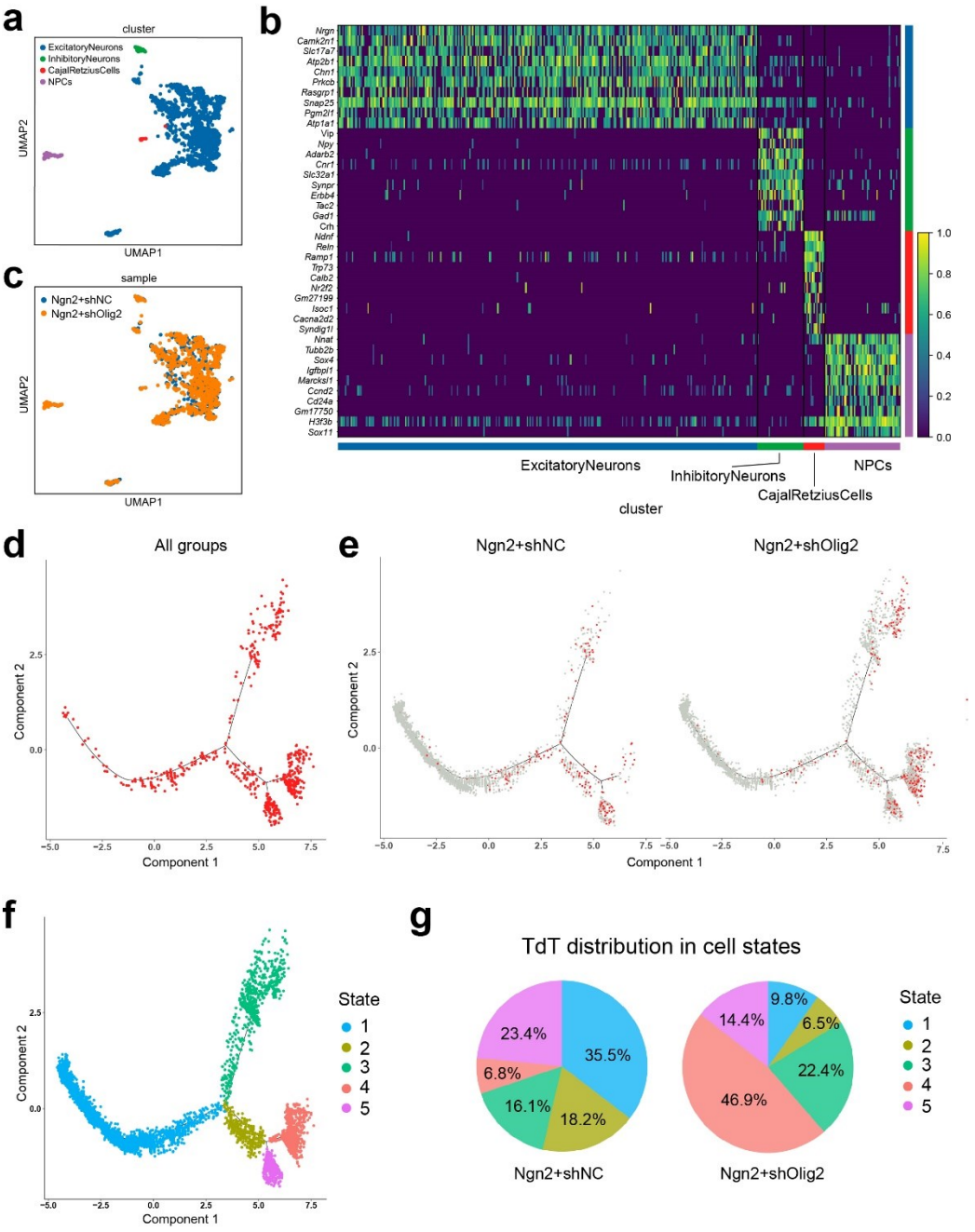

Supplementary figure 12. Cell fate alternation after Olig2 knockdown

a, UMAP showing sub-clusters of neurons. **b,** Heatmap depicting the differentially expressed marker genes in different neuron sub-clusters. **c,** Cell clusters of the Ngn2+shNC and the Ngn2+shOlig2 groups. Note that more NPCs in the Olig2 knockdown group (n = 43) than that in the shNC group (n = 11). **d,** tdT projection to the pseudotime trajectory. **e,** tdT projection to the pseudotime trajectory from the Ngn2+shNC group (left) and the Ngn2+shOlig2 group (right), respectively. **f,** Trajectory plot by cell states. **g,** Comparison of tdT distribution in cell states between the two groups.

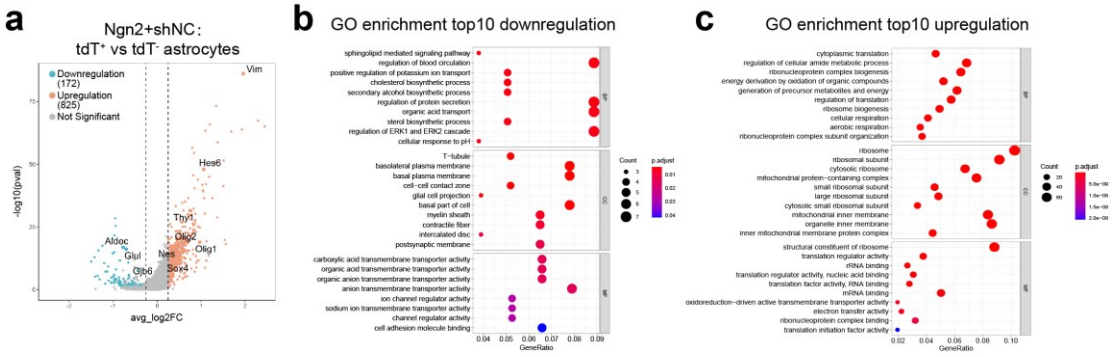

Supplementary figure 13. Ngn2 induces transcriptome alteration in astrocytes

a, Volcano plot showing DEGs between tdT^+ and tdT^- astrocytes in the Ngn2+shNC group. **b,** Top 10 GO enriched downregulated pathways. **c,** Top 10 GO enriched upregulated pathways.

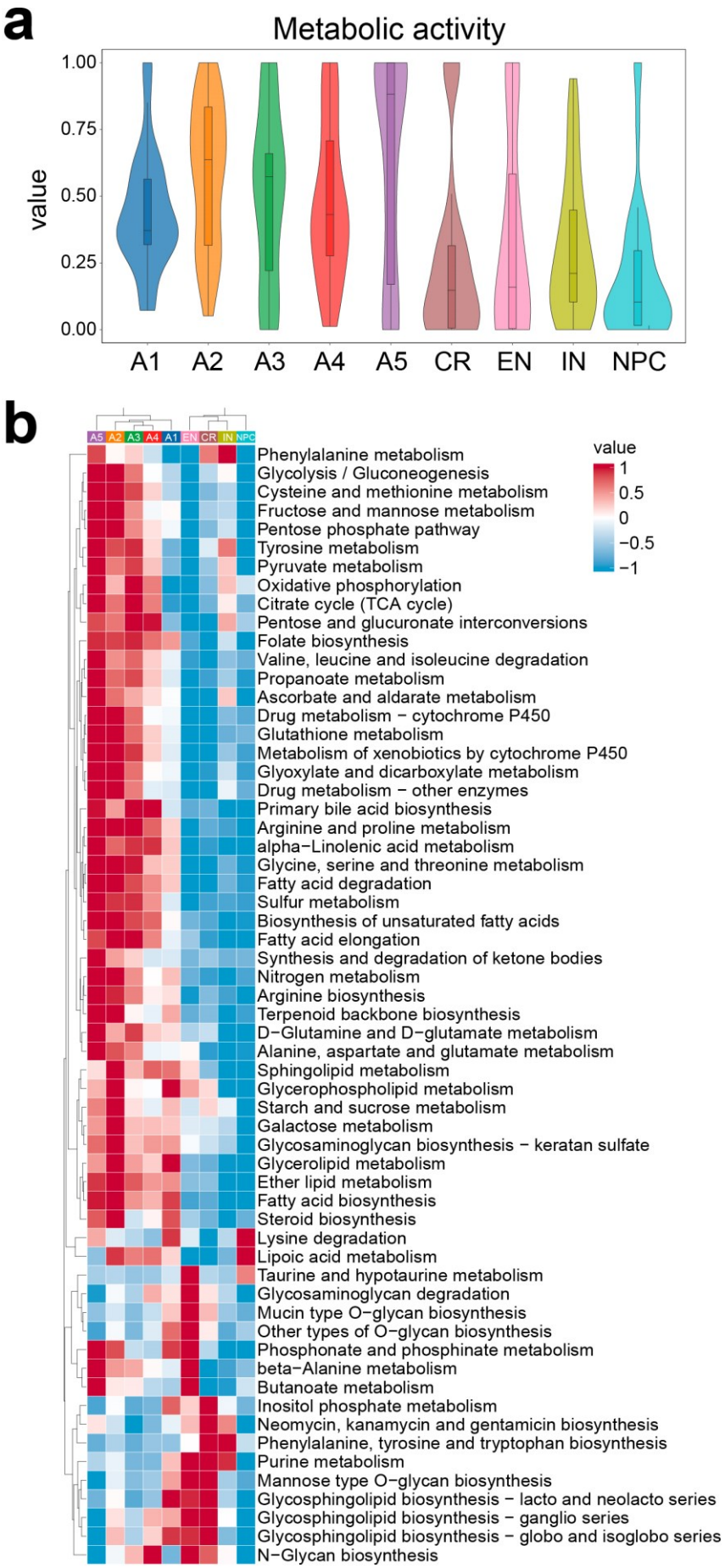
a
Metabolic activity
value
1.00
0.75
0.50
0.25
0.00
A1
A2
A3
A4
A5
CR
EN
IN
NPC
b
A5
A2
A3
A4
A1
EN
CR
IN
NPC
value
1
0.5
0
−0.5
−1
Phenylalanine metabolism
Glycolysis / Gluconeogenesis
Cysteine and methionine metabolism
Fructose and mannose metabolism
Pentose phosphate pathway
Tyrosine metabolism
Pyruvate metabolism
Oxidative phosphorylation
Citrate cycle (TCA cycle)
Pentose and glucuronate interconversions
Folate biosynthesis
Valine, leucine and isoleucine degradation
Propanoate metabolism
Ascorbate and aldarate metabolism
Drug metabolism − cytochrome P450
Glutathione metabolism
Metabolism of xenobiotics by cytochrome P450
Glyoxylate and dicarboxylate metabolism
Drug metabolism − other enzymes
Primary bile acid biosynthesis
Arginine and proline metabolism
alpha−Linolenic acid metabolism
Glycine, serine and threonine metabolism
Fatty acid degradation
Sulfur metabolism
Biosynthesis of unsaturated fatty acids
Fatty acid elongation
Synthesis and degradation of ketone bodies
Nitrogen metabolism
Arginine biosynthesis
Terpenoid backbone biosynthesis
D−Glutamine and D−glutamate metabolism
Alanine, aspartate and glutamate metabolism
Sphingolipid metabolism
Glycerophospholipid metabolism
Starch and sucrose metabolism
Galactose metabolism
Glycosaminoglycan biosynthesis − keratan sulfate
Glycerolipid metabolism
Ether lipid metabolism
Fatty acid biosynthesis
Steroid biosynthesis
Lysine degradation
Lipoic acid metabolism
Taurine and hypotaurine metabolism
Glycosaminoglycan degradation
Mucin type O−glycan biosynthesis
Other types of O−glycan biosynthesis
Phosphonate and phosphinate metabolism
beta−Alanine metabolism
Butanoate metabolism
Inositol phosphate metabolism
Neomycin, kanamycin and gentamicin biosynthesis
Phenylalanine, tyrosine and tryptophan biosynthesis
Purine metabolism
Mannose type O−glycan biosynthesis
Glycosphingolipid biosynthesis − lacto and neolacto series
Glycosphingolipid biosynthesis − ganglio series
Glycosphingolipid biosynthesis − globo and isoglobo series
N−Glycan biosynthesis

Supplementary figure 14. Olig2 downregulation facilitates metabolic alteration in astrocyte

a, Violin plot showing metabolic activity between different subclusters of astrocytes and neurons. **b,** Gene set scoring showing diverse metabolic pathway activities in astrocyte and neuron subclusters.

a

Olig2 binding motifs in astrocytes

Rank	Motif_Top 10	P-value	Rank	Motif_Top 10	P-value
1	*Sp1 (Zf)*	1e-45	6	*Nfy (CCAAT)*	1e-11
2	*Bpc6 (Bprbpc)*	1e-21	7	*Klf3 (Zf)*	1e-10
3	*Frs9 (Nd)*	1e-18	8	*Sp5 (Zf)*	1e-10
4	*Klf15 (Ma1513.1)*	1e-15	9	*Klf1 (Zf)*	1e-9
5	*Klf10 (Zf)*	1e-14	10	*Sp2 (Zf)*	1e-7

Supplementary figure 15. Olig2 binding targets in Ngn2-tdT astrocytes

a, Known motif analysis of Olig2-binding regions (top 10) in Ngn2-overexpressing astrocytes. Note that Canonical E-box (CAGCTG) was not found to be enriched in astrocytes.

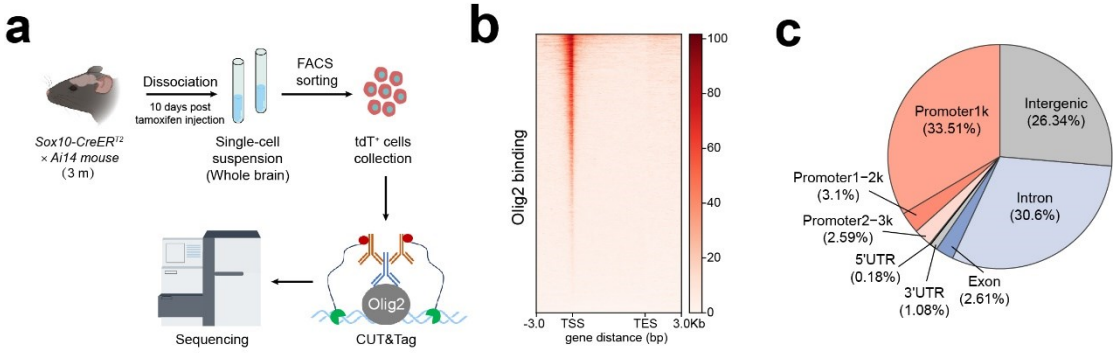

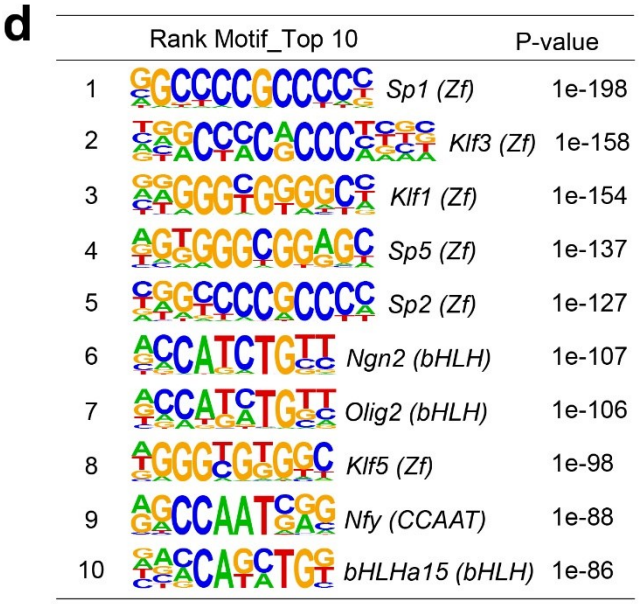

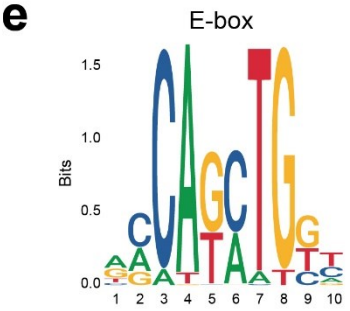

Supplementary figure 16. Olig2 binding targets in oligodendrocyte lineage cells

a, Experimental workflow of CUT&Tag analysis to assess Olig2 binding profiles in FACS purified tdT$^+$ oligodendrocyte lineage cells from adult Sox10-CreER^{T2} × Ai14 mouse brain. Two replicate experiments were involved in this study. Created in BioRender.com. Hou, KY. (https://BioRender.com/dqedntv). **b,** Heatmap showing Olig2-binding signals. **c,** Pie chart illustrating the genomic distribution of CUT&Tag peaks. **d,** Known motif analysis of Olig2-binding regions (top 10) in oligodendrocyte lineage cells. **e,** Canonical E-box (CAGCTG) was found to be enriched in Olig2 CUT&Tag of oligodendrocyte lineage cells.

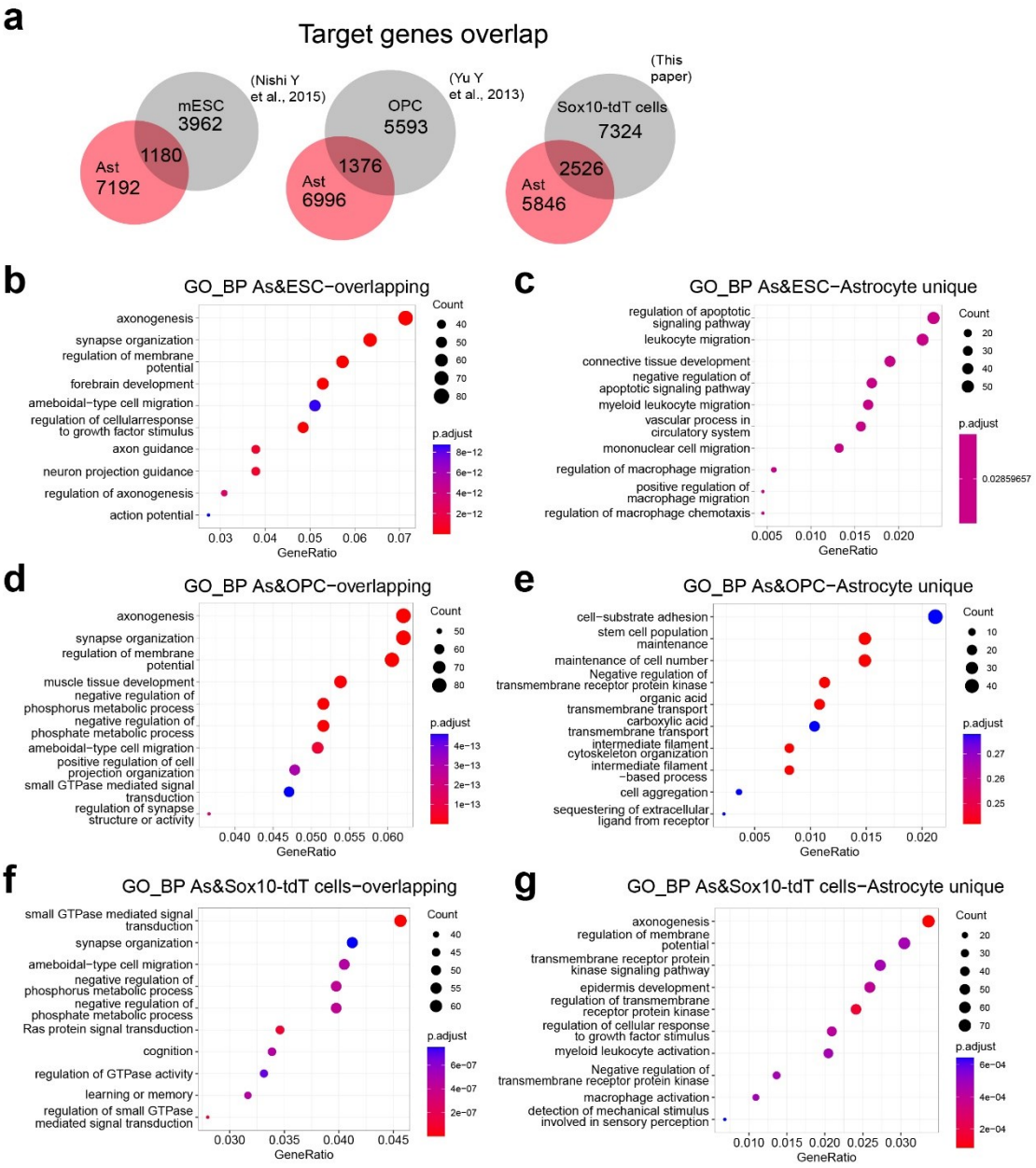

Supplementary figure 17. GO analysis reveals Olig2-regulating pathways in Ngn2-overexpressing astrocytes.

a, Venn diagram showing overlap of Olig2 occupancy between astrocytes and mESCs or OPCs or Sox10-tdT cells, respectively. **b,** Top10 GO-BP showing enriched pathways of Olig2-targeted overlapping genes between Ngn2-overexpressing astrocytes and ESCs. **c,** Top10 GO-BP showing enriched pathways of Olig2-targeted genes unique to Ngn2-overexpressing astrocytes compared with those of ESCs. **d,** Top10 GO-BP showing enriched pathways of Olig2-targeted overlapping genes between Ngn2-overexpressing astrocytes and OPCs. **e,** Top10 GO-BP showing enriched pathways of Olig2-targeted genes unique to Ngn2-overexpressing astrocytes compared with those

of OPCs. **f,** Top10 GO-BP showing enriched pathways of Olig2-targeted overlapping genes between Ngn2-overexpressing astrocytes and adult mouse Sox10-tdT cells. **g,** Top10 GO-BP showing enriched pathways of Olig2-targeted genes unique to Ngn2-overexpressing astrocytes compared with those of Sox10-tdT cells.

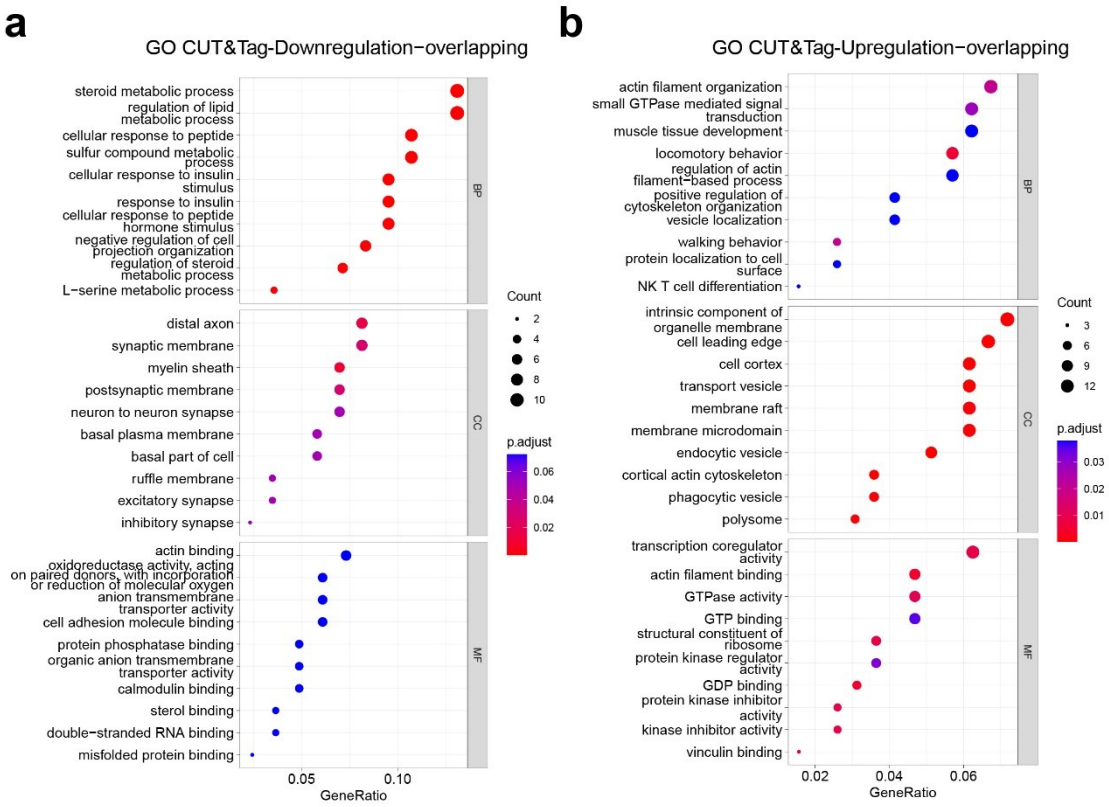

Supplementary figure 18. GO analysis reveals Olig2 directly regulating pathways

a, Top10 GO analysis showing enriched pathways of Olig2-targeted genes with transcriptional downregulation in scRNA-seq. **b,** Top10 GO analysis showing enriched pathways of Olig2-targeted genes with transcriptional upregulation in scRNA-seq.